JOURNAL OF PROPULSION AND POWER
Vol. 11, No. 3, May–June 1995

Solid Rocket Motor Internal Flow During Ignition

W. A. Johnston*
The Aerospace Corporation, El Segundo, California 90245

A numerical procedure is presented for the analysis of the internal flow in a solid rocket motor (SRM) during the ignition transient period of operation, along with the results obtained when this computer code was applied to several motors. The purpose of this code development effort was to achieve a detailed picture of the unsteady flowfield for a SRM of arbitrary design during this period of ignition delay, propellant ignition, flame spreading, and chamber filling/pressurization. The approach was to combine an unsteady, axisymmetric solution of the equations of inviscid fluid motion (Euler equations) with simple models for the convective and radiative heat transfer to the propellant surface during the run up to ignition. An unsteady, one-dimensional heat conduction solution for the propellant grain is coupled to this unsteady flow solution in order to calculate the propellant surface temperature. This solution, together with a surface temperature ignition criterion, determines the ignition delay and flame spreading. First, data were used from a Titan 5-1/2-segment solid rocket motor static firing to fix an unknown constant in the heat transfer model. Then, the computer code was applied to two solid rocket motors, Titan 7-segment and Space Shuttle, for which time-dependent chamber pressure measurements were available from static firings. Good agreement with the data was obtained.

Introduction

A DETAILED picture of the situation internal to a solid rocket motor (SRM) during the ignition transient period of operation is of interest for several reasons. For example, consider the ignition overpressure phenomenon that attends the launch of any vehicle with SRMs. Here, the pressure waves that emerge from the SRM nozzles into the surrounding air during the first second after ignition reflect off the vehicle and ground structures, placing structural demands on them. These overpressure waves are the result of the rapid rise in chamber pressure that occurs during this period. An analysis of this phenomenon (e.g., see Ref. 1) requires a knowledge of how the mass flow rate through the nozzle varies with time; this, in turn, requires a knowledge of the chamber pressure and temperature history. A numerical procedure, such as the one described in this article, supplies this information. As another example, consider the time-dependent pressure loads that a propellant grain experiences in a segmented SRM. An analysis of this load history is possible only if one possesses a detailed knowledge of the unsteady, internal SRM flowfield. Finally, a numerical procedure of this type could be used to investigate the adequacy of a particular igniter for a given SRM. The methods currently used to model an internal SRM flowfield during the ignition transient period can be categorized as either control volume (lumped parameter) or one-dimensional analyses. An overview of these methods, as well as other material related to the analysis of SRM ignition transients, may be found in Refs. 2 and 3.

In this article, a numerical procedure is presented for the analysis of the internal flow in an SRM during the ignition transient period of operation, along with the results obtained by applying this computer code to several SRMs. The purpose of this code development effort was to achieve a detailed picture of the unsteady flowfield for an SRM of arbitrary design during this period of ignition delay, propellant ignition, flame spreading, and chamber filling/pressurization. The approach was to combine an unsteady, axisymmetric solution of the equations of inviscid fluid motion, with simple models for the convective and radiative heat transfer to the propellant surface during the run up to ignition. This inviscid flow solution consists of a time-marching, finite volume solution of the Euler equations that spatially is second-order accurate. A code employing the total variation diminishing (TVD) methodology of Harten[4] has been developed for the analysis of geometrically complicated flowfields[5,6]; a version of this code, tailored to the internal flow in an SRM, was used in this study. While the form of the convective and radiative heat transfer modeling purposely was kept quite simple, it soon became apparent that the ability of the code to make accurate predictions was extremely sensitive to the expression for heat transfer from the gas to the propellant surface. For this reason, data from a Titan 5-1/2-segment SRM static firing were used to help fix a final expression for the radiative heat transfer. An unsteady, one-dimensional heat conduction solution for the propellant grain is coupled to the unsteady flow solution in order to calculate the propellant surface temperature. This solution, together with a surface temperature ignition criterion, determines the ignition delay and flame spreading rate. During an ignition transient simulation, the internal SRM flowfield geometry is held fixed. Since grain deformation can significantly alter the internal geometry,[7] and since there is a rapid increase in the pressure load on the propellant at this time, certain SRMs may exhibit a strongly time-dependent internal flowfield geometry during the ignition transient. The fixed grain geometry calculations described in this article are valid only if the propellant deformation is small, due to a stiff (high modulus) propellant or to the nature of the grain design. In cases where the grain deformation is not small, such fixed geometry calculations can provide only a preliminary assessment of SRM performance. A coupled flow-structural interactive calculation is needed in the final analysis. However, it should be added that the present axisymmetric ignition transient calculation, which provides a better picture of the surface pressure distributions on propellant segments than can one-dimensional or control volume analyses, could be used as the basis for an interactive calculation of that type.

The computer code was applied to a Titan 7-segment SRM and a Space Shuttle SRM, for which time-dependent chamber pressure measurements were available from static firings. Good agreement with the data was obtained.

Presented as Paper 91-1655 at the AIAA 22nd Fluid Dynamics, Plasmadynamics, and Lasers Conference, Honolulu, HI, June 24–27, 1991; received Feb. 3, 1992; revision received Oct. 16, 1994; accepted for publication Oct. 16, 1994.

*Member of Technical Staff. Member AIAA.

Theory

As stated previously, the numerical procedure used in this study has essentially three components: 1) an unsteady internal flow solution, 2) expressions for the heat transfer to the propellant surface prior to ignition, and 3) an unsteady heat conduction solution for the propellant surface temperature.

As such, the methodology of this study is similar to that of Peretz et al.[8]; it is instructive to point out the major differences between the present study and Ref. 8. First, the flow solution is axisymmetric in the present study, one dimensional in the previous work. Second, in the present study, expressions for the heat transfer are formulated with the help of SRM experimental data, and radiation is included in the heat transfer model. Radiation is especially important in our numerical model, because the extension to an axisymmetric flow solution means that the flow and flame situation inside the propellant slots is to be analyzed, where the low gas velocity suggests that convection will play a diminished role, and because the combustion gas in the motors considered here is laden with alumina particles and has a high emissivity. The component parts of this coupled, time-dependent numerical procedure for the ignition transient period now are discussed separately.

Flow Solution

The inviscid, axisymmetric, single-phase flow solution performed in this study consists of a time-marching, finite volume solution of the Euler equations by a numerical procedure described in detail in Ref. 5. The TVD methodology used in this numerical procedure ensures that the flow solution is spatially second-order accurate, and that flowfield discontinuities (shocks, contact surfaces) are resolved without wiggles or excessive smearing. The finite volume cell mesh used for the Titan 5-1/2-segment SRM, which is shown in Fig. 1, is typical of the grids used in this study. The cell mesh runs the length of the motor from the head end to a short distance downstream of the nozzle throat. In the radial direction, the mesh extends from the igniter wall at the head end or the motor centerline in the rest of the motor, out to the propellant surface or the slot/nozzle walls. An axisymmetric geometry allows for the resolution of the slots between propellant segments, but does not allow us to account directly for such three-dimensional features as a canted nozzle or axial grooves in a star-grained forward closure. Both features appear in the Titan 5-1/2-segment SRM. The approach to these difficulties taken in this study has been to disregard the nozzle cant while maintaining the correct throat area, and to omit the axial grooves from the propellant geometry while increasing the burn rate in the forward closure to account for the missing burn area. In some of the motors considered, an environmental seal or plug initially is placed in the nozzle downstream of the throat; this seal bursts as the pressure of the motor rises. The computational approach here was to place a solid barrier along a radial grid line in the nozzle to simulate the seal and to have the barrier disappear at a pressure differential of 1 atm to simulate the burst.

Several types of boundary conditions are encountered in these calculations on the boundary of the computational domain. First, consider the outflow portion of the boundary downstream of the nozzle throat. This is a subsonic outflow boundary initially, but it soon becomes a supersonic outflow boundary as the exhaust velocity increases. The numerical approach to the treatment of this portion of the boundary is first to affix an additional column of cells to the mesh. Then, if the outflow is subsonic, so that the mathematical problem requires one boundary condition, the pressure is set at atmospheric and zero-order extrapolation of the entropy, flow angle, and outgoing Riemann Invariant, completes the specification in these cells. If the outflow is supersonic, the mathematical problem requires no boundary conditions, and all flow variables are extrapolated from upstream. A better approach in dealing with a subsonic outflow boundary would have been to locate the boundary at the nozzle exit plane or at some distance outside the nozzle. However, since the nozzle chokes and the exit flow goes supersonic rather quickly in an SRM, this method of simplifying and economizing the present calculation was considered to be reasonable. This is true especially for motors with an environmental seal, since the exit flow goes supersonic very soon after the seal bursts.

A third type of boundary condition that occurs is the case of an impermeable boundary, which arises at solid walls. Solid walls include the motor casing (in slots and at the head end), restrictors, igniter wall, nozzle wall, environmental seal, and the propellant surface prior to ignition. Impermeability is the only mathematical requirement at this type of boundary. This requirement is met with a simple model based on symmetric, reflecting shock or rarefaction waves of equal strength. Since the mass, momentum, and energy flux through a solid surface all are zero, it remains only to determine the pressure at this surface, which is accomplished in the following manner. Let p_c, ρ_c, a_c, and u_c represent the pressure, density, sound speed, and fluid velocity normal to the wall (positive toward the wall) in a cell adjacent to the wall at time $t = 0$. If u_c is positive, then a shock wave propagates away from the wall for $t > 0$. If u_c is negative, then a rarefaction wave propagates away from the wall for $t > 0$. In the first case, standard formulas

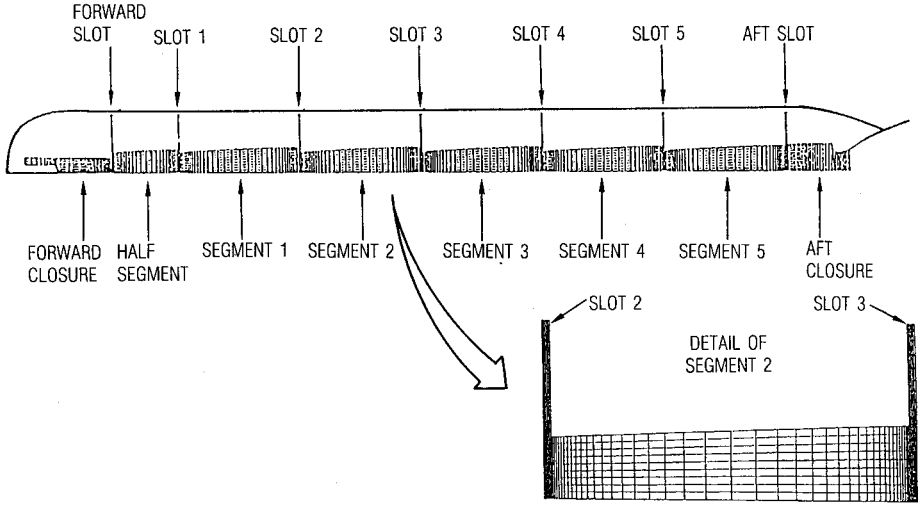

Fig. 1 Cell mesh for the Titan 5-1/2-segment SRM internal flowfield.

(e.g., see Ref. 9, Section 67) give the following expression for the wall pressure:

$$\frac{P_{\text{wall}}}{p_c} = 1 + \frac{\gamma(\gamma+1)}{4}\frac{u_c^2}{a_c^2}\left\{1 + \left[1 + \frac{16a_c^2}{(\gamma+1)^2u_c^2}\right]^{1/2}\right\} \quad (1)$$

where γ is the specific heat ratio. In the second case

$$\frac{P_{\text{wall}}}{p_c} = \left[1 + \frac{(\gamma-1)}{2}\frac{u_c}{a_c}\right]^{2\gamma/(\gamma-1)} \quad (2)$$

A fourth type of boundary condition encountered is the case of a subsonic inflow boundary, which occurs at burning propellant surfaces. Here we set three boundary conditions for our system of four governing equations. First, the stagnation enthalpy of the combustion gas coming off the burn surface is specified. Second, we use a relation between the mass flow rate and the pressure at the burning surface

$$(\rho u)_{\text{surface}} = \rho_{\text{prop}} K(p_{\text{surface}}/1000)^n \quad (3)$$

where p is in psi, ρu is in lbm/in.^{2}-s, ρ_{prop} is the propellant density, (lbm/in.^{3}), K is the burn rate constant, (in./s), and n is the burn rate exponent. Finally, the mass injection is taken to be normal to the surface. The numerical approach implemented in the case of a subsonic inflow boundary follows Ref. 10. Notice that the burn surface model does not include erosive burning. Earlier in the development of this computer code, an erosive burning model of the Lenoir-Robillard type[11] was included in the program. However, some initial test runs for the Titan 5-1/2-segment SRM indicated that its effect on this motor was slight, while its inclusion in the code resulted in a noticeable increase in computational expense. Therefore, erosive burning has been neglected for the motors considered in this study. It would be fairly simple to reintroduce this to the code, if the need was deemed sufficient.

A fifth type of boundary condition encountered is the case of a supersonic inflow boundary, which occurs at the igniter port. We note that the flow from a typical pyrogenic igniter used in the Titan and Space Shuttle SRMs is not instantly supersonic, but it must rise to this level over a small but finite time interval in the same way that the SRM itself achieves a supersonic exhaust velocity. However, we ignore this time interval, which is small even in comparison with the ignition transient period, and assume from the onset that this flow is supersonic. At a supersonic inflow boundary, the mathematical requirement is to specify completely the incoming flow. This is accomplished in the following manner. First, the inflow stagnation temperature is specified. Second, the igniter mass flow rate as a function of time is supplied to the code in tabular form. Third, the inflow is assumed normal to the boundary. If the port area is taken as the throat area, then standard one-dimensional isentropic formulas can be used to calculate the stagnation pressure and to complete the inflow specification.

The flow solution is initiated by setting the pressure and temperature at their ambient values, setting the velocity at zero, and starting the igniter mass flow. The combustion gas values for the gas constant R, and the specific heat ratio γ, are used throughout the solution. Even if the igniter and the motor gas are assumed the same, an assumption that was made for all the motors in this study, the use of these values for R and γ ignores the air that originally fills the motor. However, this air is flushed out of the motor very quickly, and so this approach was considered to be a reasonable approximation when the entire ignition transient period is considered.

Heat Transfer Model

The heat transfer to the propellant surface is assumed to result from convection and radiation, and we have attempted to model both processes. Our goal in formulating the heat transfer coefficients was to use very simple models for the convective and radiative heat transfer and, where necessary, to add to these expressions undetermined coefficient(s) that could be adjusted to bring the numerical results into agreement with static firing data. The coefficient(s), once set, should remain unchanged thereafter.

For the local convective heat transfer coefficient, we employ the expression

$$h_c = (0.023)Pr^{-2/3}c_p(\mu/D)^{0.2}(\rho v)^{0.8} \quad (4)$$

where

c_p = specific heat, constant pressure
D = reference length
Pr = Prandtl number
r = recovery factor ($r = Pr^{1/3}$)
T_{af} = average film temperature [$T_{\text{af}} = \frac{1}{2}(T_{\text{aw}} + T_{\text{wall}})$]
T_{aw} = adiabatic wall temperature ($T_{\text{aw}} = T + rv^2/2c_p$)
T_{wall} = wall temperature
μ = gas viscosity [$\mu = \mu_{\text{ref}}(T_{\text{af}})^{0.65}$ with T_{af} in °R]
ρ, T, v = gas density, temperature, and velocity in the adjacent cell

This expression essentially is a standard formula for the turbulent, convective heat transfer in a tube (e.g., see Ref. 12, Sec. 8.3). For surfaces in the bore of the motor, the local bore diameter is used for the reference length D. In the slots, which are confined regions, the surface heat transfer and flame speed proved to be fairly insensitive to the choice of convective heat transfer model. Since the gas velocity ahead of the flame front in these areas (i.e., at the top of the slots) was very low, this result seemed reasonable. Due to the diminished importance of convective heat transfer here, we continue to use Eq. (4) for simplicity, with the slot width as the reference length D. Convection is an important factor near the mouth of the slots, but radiation appears to be largely responsible for heating the propellant and advancing the flame far inside the slots.

The radiative heat transfer model used in this study was as follows. For surfaces in the bore of the motor, consider an unignited propellant surface area element, above which there is hot combustion gas densely filled with aluminum particles. A view factor of 1 for the surface area element leads to the following expression for the radiative heat transfer coefficient (e.g., see Ref. 12, Chap. 5)

$$h_r = C_{\text{sf}}\sigma(T^2 + T_{\text{wall}}^2)(T + T_{\text{wall}}) \quad (5)$$

where σ is the Stefan-Boltzman constant and C_{sf} is an empirical coefficient, that we have set from static firing data at (0.25). The factor C_{sf} is expected to account for transfer factors, such as gas emissivity, gas transmissivity, and surface absorptivity, the combined effect of which is difficult to estimate.

Our early experience in running this code with the convective and radiative heat transfer modeling described so far, indicated that the flame, which ran the length of the bore rather quickly for these motors (in about 150 ms), was unable to completely penetrate the slots by the time 500 ms had elapsed. This seemed unrealistic; also, comparisons with measured chamber pressure histories indicated that the code was too slow in reaching the steady pressure value. For these reasons, it was necessary to employ an enhanced radiative heat transfer coefficient in the slots. Since the radiative heat transfer model just described makes no allowance for the proximity of the advancing flame front, which would cause an increase in h_r, this refinement seemed warranted.

The radiative heat transfer model used in the slots was as follows. Consider the heating of a small portion of the unignited propellant surface that lies adjacent to burning propel-

lant, and assume that this neighboring flame extends in a direction perpendicular to the surface for a distance that is large compared to the size of that portion of the unignited surface under consideration. This arrangement implies a flame view factor of $\frac{1}{2}$ for the unignited surface area element. If we further assume that the propellant surface absorbs and the flame emits perfectly, then the following expression for the radiative heat transfer coefficient (e.g., see Ref. 12, Chap. 5) is obtained

$$h_r = \tfrac{1}{2}\sigma(T_{\text{flame}}^2 + T_{\text{wall}}^2)(T_{\text{flame}} + T_{\text{wall}}) \qquad (6)$$

where T_{flame} is the flame temperature. We have employed this expression, augmented by a contribution from the remainder of the view field [given by Eq. (5) with a factor of $\frac{1}{2}$ inserted], to calculate the radiative heat transfer to the propellant surface area element that lies adjacent to the advancing flame front. We ignore the radiative contribution of the flame for surface area elements that lie farther ahead of the flame. This procedure may overestimate the heat transfer to the propellant surface area element adjacent to the advancing flame front, and underestimate the temperature rise ahead of that area element, somewhat. It would be possible to refine the procedure used here, but the results of the present study did not indicate that this was necessary. Furthermore, when this method of augmenting h_r to account for the proximity of the flame front was employed in the bore where the calculated rate of flame spread was already quite fast, the effect on the calculated chamber pressure and temperature histories was negligible, and so even this refinement was used only in slot regions.

With the current method, it was found that the flame would completely penetrate the slots in a reasonable time period (typically by the time 300 ms had elapsed), and comparisons with measured chamber pressure histories yielded good agreement.

Propellant Surface Temperature Solution

An unsteady, one-dimensional heat conduction solution for the propellant temperature distribution normal to the surface is used to determine the surface temperature. Our approach utilizes an exact solution of this initial/boundary value problem, although there are other ways to proceed (e.g., see Ref. 3). For a semi-infinite region, initially at uniform temperature and subjected to a specified heat flux at the boundary, the boundary temperature is given by[13]

$$T_{\text{wall}}(t) = T_p + \sqrt{\frac{\alpha}{\pi}} \int_0^t \frac{q(\tau)}{k} \frac{d\tau}{\sqrt{t - \tau}} \qquad (7)$$

where

k = thermal conductivity of propellant
T_p = initial propellant temperature
q = total heat flux [$q = h_c(T_{\text{aw}} - T_{\text{wall}}) + h_r(T - T_{\text{wall}}) + h_{r'}(T_{\text{flame}} - T_{\text{wall}})$]
α = thermal diffusivity of propellant

If the time integral is subdivided into (n) time steps, and the heat flux after (i) time steps [$q_i = q(t_i)$] is held constant for the ($i + 1$) time step, then the following expression for the wall temperature results

$$T_{\text{wall}}(t_n) = T_p + 2\sqrt{\frac{\alpha}{\pi}} \sum_{i=0}^{i=n-1} \frac{q_i}{k} (\sqrt{t_n - t_i} - \sqrt{t_n - t_{i+1}}) \qquad (8)$$

This equation is time marched in conjunction with the flow solution, although a larger time step is used here.

Table 1 Gas and propellant properties

	Titan 5-1/2-segment	Titan 7-segment	Space Shuttle SRM
γ	1.18	1.18	1.14
R, ft²/s²-°R	1830.0	1808.0	1729.0
T_{flame}, °R	5950.0	5950.0	5718.0
T_{ignition}, °R	1260.0	1260.0	1260.0
ρ_{prop}, lbm/in.³	0.0635	0.0635	0.06347
K, in./s	0.354*	0.328	0.44
n	0.273	0.20	0.35
α, in.²/s	3.153×10^{-4}	3.153×10^{-4}	3.153×10^{-4}
Pr	0.45	0.45	0.45
k, Btu/in.-s-°R	6.088×10^{-6}	6.088×10^{-6}	6.088×10^{-6}
μ_{ref}, slugs/ft-s	6.55×10^{-9}	6.55×10^{-9}	7.02×10^{-9}

*This value is discussed in the section entitled Numerical Results.

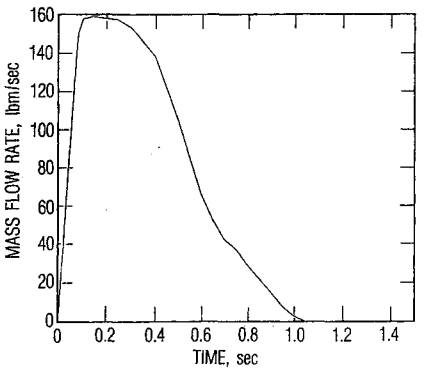

Fig. 2 Igniter mass flow rate, Titan 5-1/2-segment SRM.

Numerical Results

The results obtained with the numerical procedure are presented in this section. Various gas and propellant properties for the three motors analyzed are found in Table 1. A typical SRM solution required about 6 h of CPU time on the Cray X-MP-14 and about 2.0 Mwords of storage for a grid mesh of 5000 cells.

Titan 5-1/2-Segment SRM

The first test case for the code was a static firing (1206-3) of the Titan 5-1/2-segment SRM.[14] Our intention was to use the data from this test case to fix the expression for the radiative heat transfer, which then would remain unchanged in all subsequent applications. The cell mesh used in the numerical solution for this motor is shown in Fig. 1, where restrictors cover the front of propellant segments 1/2, 1, 2, 3, 4, and 5.

The forward closure in the Titan 5-1/2-segment SRM has a star-grain cross section, with an actual burning area that is 2.97 times larger than the burning area in our axisymmetric model. To account for this disparity, the burn rate constant K is increased by a factor of 2.97 in the forward closure.

The igniter mass flow rate used in this calculation is found in Fig. 2. A comparison of the head end chamber pressure histories from the numerical solution and the static firing experimental data is shown in Fig. 3. It must be emphasized that the excellent agreement in Fig. 3 is the end result of an iterative process that involved adjusting the value of the coefficient C_{sf} in Eq. (5), running the calculation, and then repeating until an acceptable level of agreement was obtained. Furthermore, in this calculation we have set the value of the burn rate constant ($K = 0.354$ in./s), based on an asymptotic value for the head end chamber pressure of 863 psia from the (1206-3) static firing. Therefore, the agreement in this test case does not constitute a validation of the code, and it should not be viewed as such. We rely on the test cases that are

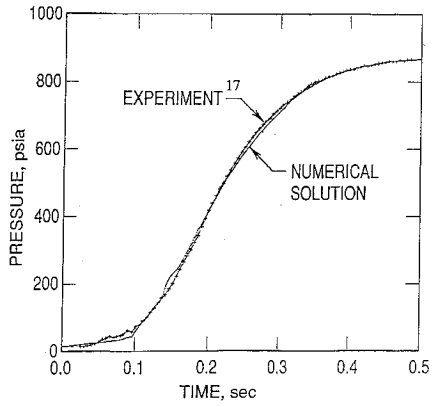

Fig. 3 Gas pressure—head end, Titan 5-1/2-segment SRM.

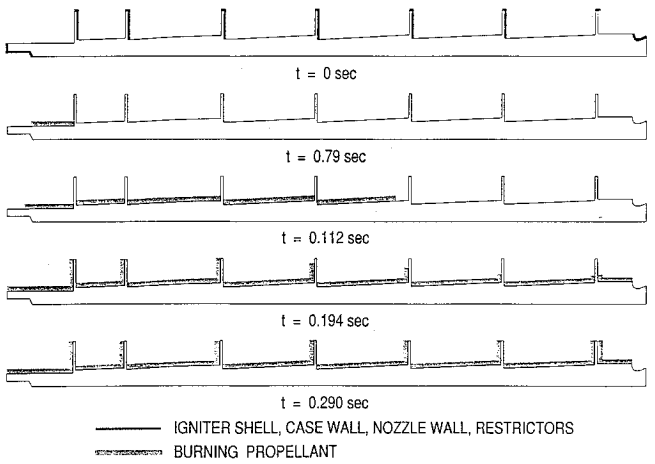

Fig. 4 Flame location—Titan 5-1/2-segment SRM.

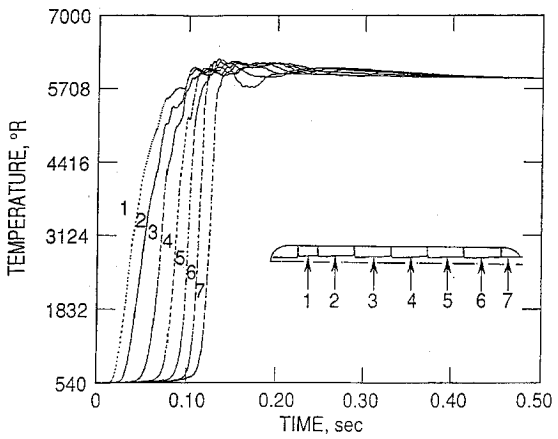

Fig. 5 Gas temperature, Titan 5-1/2-segment SRM.

discussed subsequently to provide this validation. The value of the present test case was in the insight it provided into the sequence of events inside a typical SRM during the ignition transient and in the fact that it provided a value for the coefficient $C_{sf} = 0.25$.

It is instructive to review the picture of the developing situation inside the SRM that the numerical solution depicts. At $t = 0$, the mass flow from the igniter, with its 30-deg angled port, begins. (Actually, there are three igniter ports, which are idealized as a single axisymmetric port in this calculation.) The first ignition of propellant occurs in the forward closure at about $t = 0.060$ s. From the location of first ignition between the igniter and the forward slot, the flame spreads down the bore toward the nozzle and up the bore toward the top of the motor. The location of the flame at various times is shown in Fig. 4. At about $t = 0.095$ s, the nozzle chokes and the rapid pressurization of the motor begins. By this time, the flame has reached propellant segment 3. Shortly thereafter ($t = 0.150$ s), the entire motor bore is burning; however, the flame has made little progress in penetrating the slots. The flame completely penetrates the forward slot at $t = 0.190$ s, slot no. 4 at $t = 0.240$ s, and the aft slot at $t = 0.290$ s. The entire propellant surface is burning at this point, but the chamber pressure continues to rise until the asymptotic level is reached. Gas temperature values from the calculations are plotted in Fig. 5 at several axial locations; no static firing data are available for comparison. It is evident from Fig. 5 that the gas temperature rises much earlier and more sharply than the pressure.

Titan 7-Segment SRM

The second test case for the code was a static firing (1207-6) of the Titan 7-segment SRM.[15] This motor is shown in Fig. 6, along with the cell mesh used in the numerical solution. Restrictors cover the front of propellant segments 1–7. The forward closure in the Titan 7-segment motor is longer than the forward closure in the Titan 5-1/2-segment motor and has a somewhat different star-grain cross section. The ratio of actual burning area to computational burning area, and the factor of burn rate increase in the forward closure, is 3.12.

An attempt was made in this test case to account for the fact that the flame must penetrate the axial grooves in the forward closure over some finite time interval; this implies that all of the burn rate increase factor of 3.12 should not be applied initially, but that it should achieve its full value over the course of this penetration time interval. If the flame advances into these axial grooves by a radiation-dominated process, similar to the way in which it penetrates the slots, then we can use the slot penetration time interval from the Titan 5-1/2-segment solution to estimate the penetration time interval for the axial grooves in the Titan 7-segment motor. Based on this reasoning, the burn rate increase factor was allowed to increase linearly with time until it attained its full value (3.12) at $t = 0.175$ s. The effect of this modeling on the chamber pressure history predicted for the Titan 7-segment motor (see Fig. 7) was a very slight delay in the pressure rise.

An environmental seal located downstream of the nozzle throat was modeled as a solid barrier that disappears when the pressure differential across the barrier reaches 1 atm. This occurs at an elapsed time of $t = 0.105$ s, and the nozzle chokes immediately thereafter. The presence of this seal has a negligible effect on the head end chamber pressure history. However, a seal of this type can have a noticeable effect on the aft end chamber pressure history, as we shall see in our discussion of the Space Shuttle SRM. The igniter used for the Titan 7-segment SRM had the same geometry and mass flow rate as the Titan 5-1/2-segment igniter.

A comparison of the head end chamber pressure histories from the numerical solution and static firing is shown in Fig. 7, and the agreement between the numerical and experimental results was judged to be reasonably good. Gas temperature values from the calculation are found in Fig. 8; no static firing data are available for comparison. As in the Titan 5-1/2-segment SRM, the temperature rises earlier and more sharply than the pressure.

Wall and centerline pressures are plotted as a function of axial position in Fig. 9, for two different times. During the first 0.150 s of motor operation, pressure waves propagate along the bore of the motor and reflect off the nozzle region and then back from the head end. However, by $t = 0.20$ s (see Fig. 9) the axial pressure distribution has attained the shape, if not the level, that it displays during the quasisteady period of operation, i.e., $t > 0.5$ s. At this time ($t = 0.20$ s),

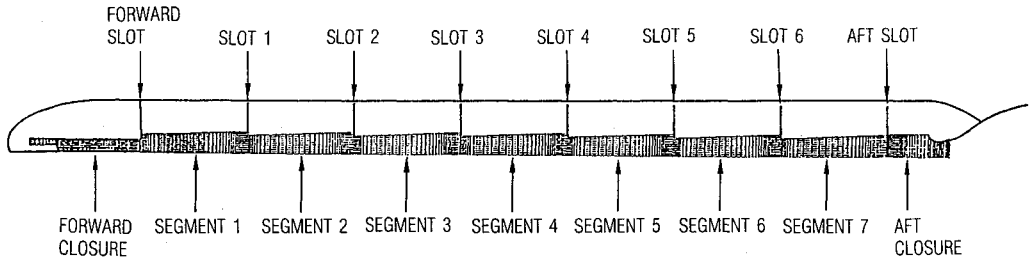

Fig. 6 Cell mesh for the Titan 7-segment SRM internal flowfield.

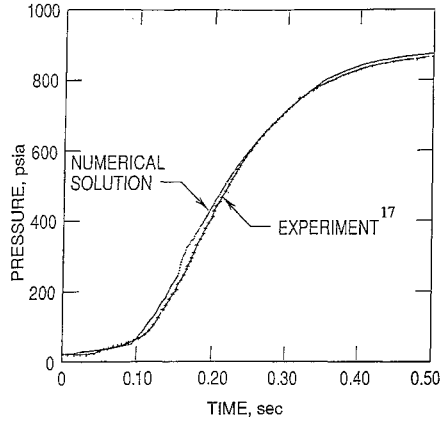

Fig. 7 Gas pressure—head end, Titan 7-segment SRM.

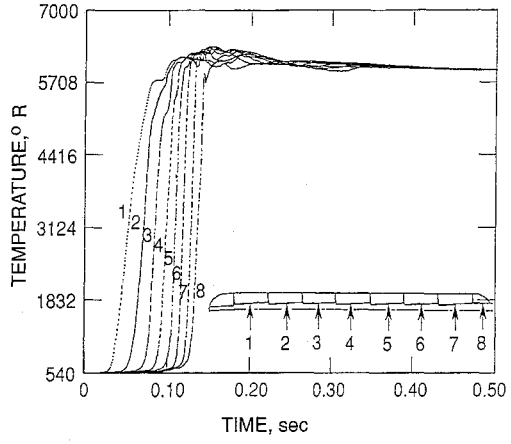

Fig. 8 Gas temperature, Titan 7-segment SRM.

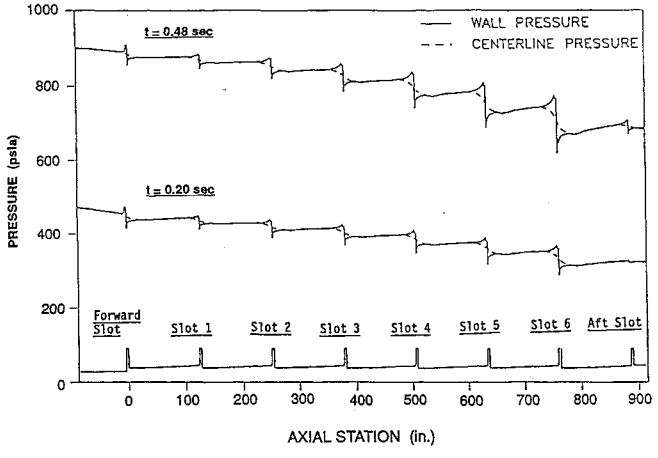

Fig. 9 Wall and centerline pressure vs axial position for two times during the ignition transient period—Titan 7-segment SRM.

most of the propellant surface is burning, although some propellant at the top of those slots at the aft end of the SRM remains unignited. The axial pressure distribution near the end of the chamber filling period (t = 0.48 s) also is shown in Fig. 9. An especially significant feature of the wall pressure curves is the large pressure drop that occurs between the top of a slot and a point just downstream of that slot on the bore surface of a propellant segment. For example, the t = 0.48 s wall pressure curve displays a 150 psi pressure difference at slot 6. This large pressure difference at slot 6 arises from the combination of a large decrease in port flow area and the high flow velocity at this site. The effect of this pressure differential acting on the forward corner of the propellant segment is to deform the corner out into the bore flow,[7] and the magnitude of this pressure differential is not apparent from the centerline pressure distribution. This demonstrates an important advantage of an axisymmetric flowfield analysis over one-dimensional and control volume methods.

Space Shuttle SRM

The third test case for the code was a static firing (QM3) of the Space Shuttle SRM.[16] The cell mesh used in the numerical solution for this motor is shown in Fig. 10. Restrictors extend radially inward from the casing wall to completely cover the front of the two center propellant segments and to partially cover the rear of the forward segment, the rear of the two center segments, and the front of the aft segment. This SRM utilizes an axial port igniter with a mass flow rate shown in Fig. 11. Since the heat transfer coefficient in this numerical procedure was calibrated for a test case with an angled igniter, it was of interest to see if the code could produce acceptable results for an SRM with an axial igniter.

In the forward propellant segment, a large portion of the propellant near the head end of the motor is configured with a star grain cross section. The ratio of actual burn area to computational burn area in this portion of the forward segment and the burn rate increase factor here is 4.57. The time interval over which the burn rate increase factor achieves its full value of 4.57 was assigned a value of t = 0.175 s. The modeling of the groove penetration process has a significant effect on the shape of the chamber pressure curves in Figs. 12–14, due to the large burn rate increase factor (4.57) in this motor. A large part of the actual burning area is hidden in our axisymmetric grid. Consequently, the numerical results are sensitive to this feature of the modeling; for this reason, the Space Shuttle SRM is a difficult test case for the code. The actual Space Shuttle SRM geometry includes a submerged nozzle, a feature that has been excluded from our grid in the interest of simplifying the geometry. This geometric omission also can be accounted for by an enhanced burn rate constant over a small portion of the geometry model's aft segment propellant surface, where the submerged region is attached in reality.

An environmental seal located downstream of the nozzle throat was modeled as a solid barrier that disappears when the pressure differential reaches 1 atm. This occurs at t = 0.078 s in the numerical solution, after which the nozzle chokes quickly. The presence of this seal causes the "spike" in the

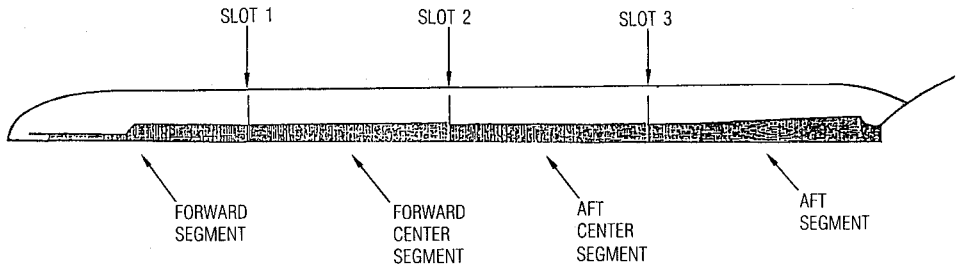

Fig. 10 Cell mesh for the Space Shuttle SRM internal flowfield.

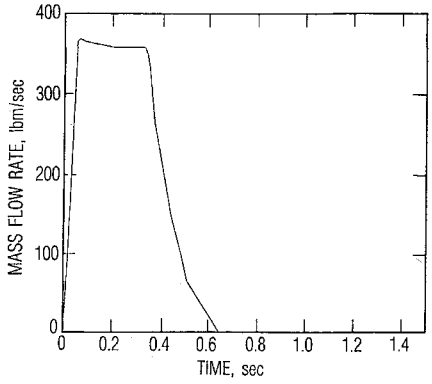

Fig. 11 Igniter mass flow rate, Space Shuttle SRM.

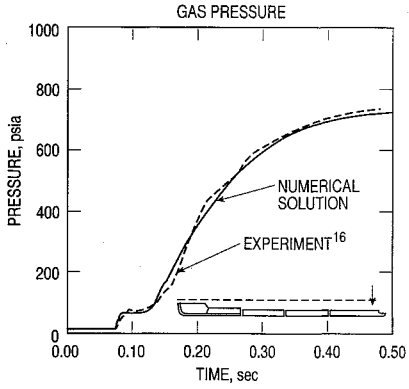

Fig. 12 Gas pressure—aft end, Space Shuttle SRM.

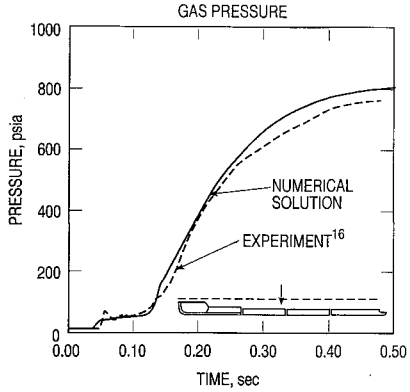

Fig. 13 Gas pressure—midmotor, Space Shuttle SRM.

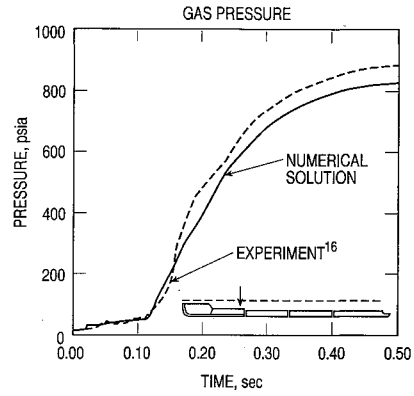

Fig. 14 Gas pressure—head end, Space Shuttle SRM.

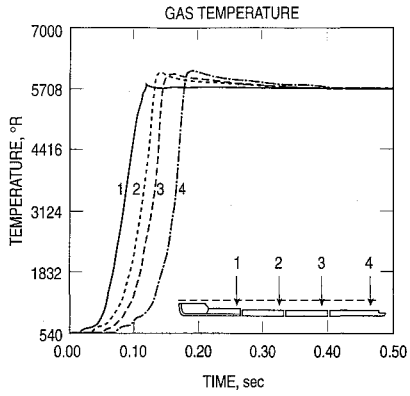

Fig. 15 Gas temperature, Space Shuttle SRM.

aft end chamber pressure (see Fig. 12), which is associated with the arrival of the igniter wave from upstream, to increase in size and definition; when the seal is removed from the calculation, this feature is much less obvious. Comparisons of chamber pressure histories from the numerical solution and the QM3 static firing are found in Figs. 12–14. The agreement is good at the aft end (Fig. 12). The agreement between the data and the numerical solution at midmotor and at the head end is only fair (see Figs. 13 and 14), and the reason for the disparity at these locations is unclear. However, given the significant three dimensionality of the grain geometry in the forward segment, it is probably unrealistic to expect close agreement at the head end. It would be possible to bring the curves into somewhat better agreement by adjusting the flame penetration time interval for the forward closure; however, it was not our intention to tune the code for this test case. Gas temperature values from the calculation are plotted in Fig. 15; no static firing data are available for comparison.

Discussion

The results presented here demonstrate the applicability of this numerical calculation procedure to the analysis of the internal flow in an SRM during the ignition transient. In the two validation test cases (Titan 7-segment, Shuttle), the agreement generally was quite good.

The numerical procedure described in this article involved a two-dimensional, unsteady flow solution coupled with a one-dimensional, unsteady heat conduction solution for the propellant grain. The surface heat transfer coefficient is assumed to depend on convection and radiation, and to be radiation dominated in the propellant slots. The expression for the radiative heat transfer coefficient [see Eq. (5)] included an

empirical coefficient C_{sf} that was set using data from the Titan 5-1/2-segment static firing; our experience was that C_{sf} could be held fixed from motor to motor with acceptable results. In conclusion, note that the three motors considered in this study all were large segmented SRMs with head end pyrogen igniters and could be characterized as similar. Therefore, prior to the application of the code to a radically different SRM design, some additional validation of the code would be appropriate.

Acknowledgments

This work was supported by the U.S. Air Force Space Systems Division under Contract F04701-88-C-0089. The author benefited from discussions with J. W. Murdock and D. L. Misterek of The Aerospace Corporation. Also, D. A. Nelson of The Aerospace Corporation made several helpful suggestions, including the approach to surface temperature evaluation. W. F. Reddall of The Aerospace Corporation suggested the numerical treatment for solid boundaries.

References

[1]Broadwell, J. E., and Tsu, C. N., "Transient Pressures Caused by Rocket Start and Shutdown in Ducted Launchers," *Journal of Spacecraft*, Vol. 4, No. 10, 1967, pp. 1323–1328.

[2]Kumar, M., and Kuo, K. K., "Flame Spreading and Overall Ignition Transient," *Fundamentals of Combustion of Solid Propellants*, Vol. 90, Progress in Astronautics and Aeronautics, AIAA, New York, 1984, pp. 305–360.

[3]Salita, M., "Rocket Propellant Ignition: A Workshop Report," *Proceedings of the 22nd JANNAF Combustion Meeting*, Vol. I, 1985, pp. 65–86.

[4]Harten, A., "High Resolution Schemes for Hyperbolic Conservation Laws," *Journal of Computational Physics*, Vol. 49, No. 3, 1983, pp. 357–393.

[5]Wang, J. C. T., and Widhopf, G. F., "A High-Resolution TVD Finite Volume Scheme for the Euler Equations in Conservation Form," AIAA Paper 87-0538; also *Journal of Computational Physics*, Vol. 84, No. 1, 1989, pp. 145–173.

[6]Ton, V. T., Wang, J. C. T., and Widhopf, G. F., "Segmented Solid Rocket Motor Internal Flow Simulations," AIAA Paper 90-0683, Jan. 1990.

[7]Glick, R. L., Caveny, L. H., and Thurman, J. L., "Internal Ballistics of Slotted-Tube Solid Propellant Rocket Motors," *Journal of Spacecraft*, Vol. 4, No. 4, 1967, pp. 525–530.

[8]Peretz, A., Kuo, K. K., Caveny, L. H., and Summerfield, M., "Starting Transient of Solid-Propellant Rocket Motors with High Internal Gas Velocities," *AIAA Journal*, Vol. 11, No. 12, 1973, pp. 1719–1727.

[9]Courant, R., and Friedrichs, K. O., *Supersonic Flow and Shock Waves*, Vol. I, Interscience, New York, 1948.

[10]Murdock, J. W., "Rocket Thrust Perturbation from Discharge of an Inert Body," *Journal of Propulsion*, Vol. 2, No. 2, 1986, pp. 117–123.

[11]Lenoir, J. M., and Robillard, G., "A Mathematical Method to Predict the Effects of Erosive Burning in Solid Propellant Rockets," *Sixth Symposium (International) on Combustion*, Reinhold, NY, 1957, pp. 663–667.

[12]Kreith, F., *Principles of Heat Transfer*, 2nd ed., International Textbook, London, 1965.

[13]Churchill, R. V., "Operational Mathematics," 3rd ed., Section 47, McGraw-Hill, 1958, p. 150.

[14]"1206-3 Static Test Report, Titan 34D Recovery Program, Phases IV and VIII," United Technologies Corp., Chemical Systems Div., CSD-4176-88-182, June 1988.

[15]"Titan IV SRM Static Test Report, 1207-5 and 1207-6," United Technologies Corp., Chemical Systems Div., CSD-4001-88-383, June 1988.

[16]Leavitt, K. H., "Space Shuttle Solid Rocket Motor, Qualification Motor Static Firing Tests," Thiokol, Wasatch Div., Test Rept. TWR-12646, June 1981.

[17]Robertson, A. F., personal communication, The Aerospace Corp., El Segundo, CA, 1988.